Spectroscopic and photoacoustic characterization of encapsulated iron oxide superparamagnetic nanoparticlesaas as a new kind of multiplatform contrast agent

Paolo Armanetti[a], Alessandra Flori[b], Cinzia Avigo[a], Luca Conti[c], Barbara Valtancoli[c], Andrea Bencini[c],Giovanni Baldi[d], Andrea Bencini[c], Luca Menichetti[a*]

[a]*Istituto di Fisiologia Clinica, CNR, Via Giuseppe Moruzzi 1, Pisa 56124, Italy;* [b]*FondazioneRegione Toscana G. Monasterio, Via Giuseppe Moruzzi 1, Pisa 56124, Italy;* [c]*Dipartimento di Chimica "Ugo Schiff", Polo Scientifico, Università degli Studi di Firenze, Via della Lastruccia 3, 50019 Sesto Fiorentino, Firenze, Italy,*[d]*Colorobbia Consulting Srl, , via Pietramarina 123, 50053 Sovigliana – Vinci, Italy.*

Abstract: Recently, a number of photoacoustic (PA) agents with increased tissue penetration and fine spatial resolution have been developed for molecular imaging and mapping of pathophysiological features at the molecular level. Here, we present bio-conjugated near-infrared light-absorbing magnetic nanoparticles as a new agent for PA imaging. These nanoparticles exhibit suitable absorption in the near-infrared region, with good photo- acoustic signal generation efficiency and high photo-stability. Furthermore, these encapsulated iron oxide nano- particles exhibit strong super-paramagnetic behavior and nuclear relaxivities that make them useful as magnetic resonance imaging (MRI) contrast media as well. Their simple bio-conjugation strategy, optical and chemical sta- bility, and straightforward manipulation could enable the development of a PA probe with magnetic and spectro- scopic properties suitable for *in vitro* and *in vivo* real-time imaging of relevant biological targets.

Keywords: Photoacoustic imaging, Optoacoustic imaging, Magnetic resonance imaging, Contrast media, Biomedical imaging, Contrast agent

1. INTRODUCTION

The laser-induced photoacoustic (PA) effect has recently been im- plemented in biomedical imaging. This effect occurs when a tissue, irra- diated with a nanosecond laser pulse, is stimulated by light absorption and produces acoustic waves due to thermo-elastic processes. The laser-induced acoustic waves generated in the tissue provide molecular information based on the optical absorption, and this information can be correlated with standard echographic images. PA imaging (PAI) is a non-ionizing imaging technique that can reveal *in vivo* features [1] at high contrast and high resolution, thereby providing different func- tional information (*i.e.* blood oxygen saturation, oxygenated-deoxygen- ated hemoglobin ratio, early angiogenic states, or hypermetabolism) [1–3]. The performance of a PA system can be enhanced by using con- trast agents [4–7], such as near-infrared (NIR) dyes and/or nanoparti- cles, that improve the sensitivity and spectroscopic specificity of a PA signal. This extends the range of applications of PAI, including the detec- tion of specific molecular targets [8].

Magnetic resonance imaging (MRI) and PAI are currently being in- vestigated for *in vivo* applications through a multimodal approach [9]. In this report, we describe the simple synthesis and characterization of a biocompatible hybrid nanosystem (also referred to as a fluorescent “nanobioreactor” or “NBRfluo”). Carboxy-terminated poly(D,L-lactide-*co*-glycolide)-*block* poly(ethylene glycol) (PLGA-b-PEG-COOH) nano- particles with an average hydrodynamic diameter of 40 nm, containing iron oxide clusters, were used as probes after loading a *de novo*-synthe- sized NIR fluorescent dye. Compared to commercial compounds, these nanoparticles exhibit super-paramagnetic behavior and nuclear relaxivities that make them promising MRI contrast agents. Here, we re- port the strategy for modular iron oxide/NIR nanoparticle synthesis and their spectral characterization, with a particular focus on multispectral PAI.

2. MATERIALS AND METHOD

Details of the synthesis and spectroscopic characterization of 6- carboxypentylamido-hexanoic fluorescein succinimidyl-ester and its magnetic resonance (MR) longitudinal and transverse relaxivities (r1and r2, in mM^{-1} s^{-1}) are reported in the Supplementary Information (SI).

2.1 Nanoplatform Synthesis

Magnetite-based nanoparticles in a polymeric matrix were synthe- sized as previously reported [10]. Briefly, 40 mL of Fe3O4 naked nano- particles suspended in diethylene glycol were sonicated for 1 h in an ultrasound bath. Then, a solution of *N*-(3.4-dihydroxyphenethyl) dodecanamide (DDA; 1.09 g, 3.2 mmol) in ethanol (120 mL) was slowly added to the glycolic suspension. The system was again sonicated for 1 h at room temperature. The Fe_3O_4-DDA suspension was diluted with 60 mL of ultrapure water, magnetically sedimented, and dispersed in 90 mL tetrahydrofuran (THF). Next, 440 mg of PLGA-b-PEG-COOH (46 kDa, 9.6 μmol) was dissolved in 10 mL THF, and this solution was then added to 90 mL of the Fe_3O_4-DDA suspension. Fluorescent nano- particles (Fe_3O_4-DDA-Fluo) were obtained by first adding a Dimethyl sulfoxide (DMSO) solution of fluorescein 488-NHS (amino reactive) to a solution of 4-aminobutylphosphonic acid (a linker that can react with the carboxyl group of the fluorochrome by its amino group and with the magnetic core by its phosphonic group); the reaction was then stirred for 3.5 h. The mixture was then added to the Fe_3O_4-DDA suspension, and the reaction was incubated overnight at room temperature. The formation of NBR was achieved by the following nanoprecipitation method: the organic phase was added to 900 mL of ultrapure water under vigorous stirring, and the water/organic ratio was maintained at 10/1 *via* the constant removal of the resulting solu- tion. The mixture was then purified by washing with phosphate-buff- ered solution, concentrated by ultrafiltration (Pellicon XL, cut-off 500 kDa) to a final volume of 150 mL [concentration of 0.3% (w/w) in Fe_3O_4], and filtered through a syringe filter (Millipore Sterivex, 0.22 μm, polyethersulfone membrane). Fluorescent NBR (NBRfluo) were prepared using the same method by substituting Fe_3O_4-DDA-Fluo (NBRfluo) for Fe3O4-DDA (NBR).

2.2 Spectroscopic Characterization

Absorption spectra were recorded on a Perkin-Elmer Lambda 25 spectrophotometer. Fluorescence emission and excitation spectra were collected on a Perkin Elmer LS55 spectrofluorimeter. HCl and/or NaOH were used to adjust the pH values of the solutions.

2.3 PA Setups

For this study, the commercial PAI system VevoLAZR (VisualSonics Inc.), which produces PA images co-registered with *B-mode* images of the surrounding structures, was used. Laser stimulation was performed in a range of wavelength windows from 680 to 970 nm in increments of 1 nm (the minimum selectable increment), and the wavelength switching time was b0.4 s. The laser illumination was transmitted to the sample by a PA probe (LZ250, VisualSonics Inc.) through an optical fiber, ending at the bottom

of the probe, in two rectangular glass win- dows placed on both sides of the echographic linear array transducer at 26 mJ (maximum deliverable energy).

The PA probe was operated in the range of 13 to 24 MHz, and the size of its field of view was on the order of 23 mm × 30 mm at an angle of 30° with the imaging plane. The axial resolution was 75 μm, while the lateral resolution was 165 μm. The acquisition time for the absorption spectrum was ∼60 s for 146 wavelengths (2-nm increment).

2.3.1 In vitro PA Setup

PA characterization was performed using a custom made phantom [11–13], consisting in a plastic box with a series of coplanar micro-medical polyethylene (PE) tubes that were non-radiopaque, non-reactive, and did not contain plasticizers [internal diameter (ID) = 860 μm, external diameter (ED) = 1320 μm]. PE was selected because it has good mechanical properties (impedance, resistance, echogenicity, *etc.*) and is easily manipulated, enabling the building of our custom setups (see Table S1 in SI for material properties). The first step in the production of the custom-made PA phantom was the preparation of samples with different dilutions of NBRfluo (Fig. 1a; stock solution, 1:2, 1:4, 1:8, 1:16). Then, five PE tubes were loaded with nanoparticles (~40 μL for each tube), and one was loaded with water for background PA estima- tion. Subsequently, the loaded PE tubes (Fig. 1b) were inserted into a plastic box through a series of keyholes and then placed under the PA probe. The box was filled with water as a probe coupling medium.

2.3.2 Ex vivo PA Setup

To achieve the characteristics of an ideal and easily reproducible phantom in biological tissue, we used a chicken breast phantom. The sample of biological tissue was placed inside the plastic box and was then covered with an agarose matrix (1%) (Fig. 1c) at a temperature of 36 °C. The box was sonicated for 15 min to remove all air bubbles. The agarose matrix is similar to water and biological soft tissue in terms of acoustic impedance and speed of sound (Table S1 in SI), guaranteeing a good acoustic coupling. Moreover, it is neutral to PA and ultrasound interactions, and it maintains the geometry of biological structures, which is important during three-dimensional acquisitions. Finally, the whole setup was filled with water at 37 °C and placed on a heated work- table to maintain a constant temperature during all PA acquisitions.

2.3.3 PA Measurements

The PA values were measured in selected regions of interest (ROIs). For the *in vitro* tests, a ROI was selected around the section of each tube corresponding to a different dilution of NBRfluo, and one around the PE tube filled with milliQ water (MQ), that was used as the background. For the *ex vivo* test, two ROIs were selected: the first one was around the injection zone of the tissue, and the second one was removed from the in- jection zone of the tissue. For each ROI, the photostability (PHSt) and PA spectral trend were studied. The PA spectrum was calculated for 146 wavelengths (2-nm intervals) in the range of 680 to 970 nm. The PHSt duration was evaluated under pulsed irradiation at 730 nm for over 1 min (around 335 laser shots). From these measurements, the relationship between PA signal and concentration was extrapolated.

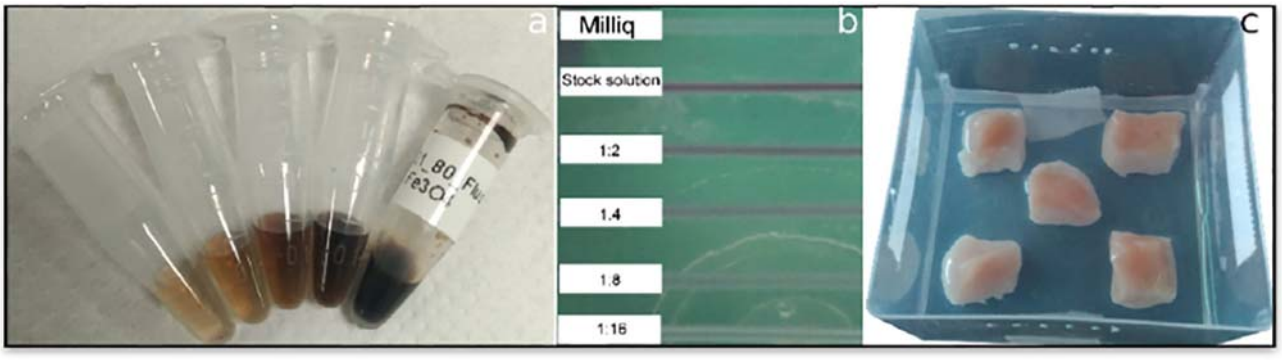

Fig. 1. (a) Different dilutions of NBRfluo, from left to right: 1:16, 1:8, 1:4, 1:2, and stock solution; (b) PE tubes loaded with different dilutions of NBRfluo; (c) *Ex vivo* setup: chicken breast pieces in agarose matrix (1%).

3. THEORY AND CALCULATIONS

Assuming that all absorbed optical energy is converted into heat and that non-thermal relaxation, such as fluorescence, is negligible for such a short laser pulse, the fractional volume expansion is negligible and the local pressure rise, P_0, produced immediately after the laser excitation can be expressed as [14]:

$$P_0 = \Gamma \text{ x } \mu a \text{ x } F \quad (1)$$

where $P0$ is the initial PA pressure due to laser excitation, Γ is the Grueneisen parameter, μ_a is the absorption coefficient, and F is the optical fluence. The PA signal is proportional to the absorbance spectrum; in fact, the absorbance, A, can be expressed as:

$$A \approx \mu a \text{ x } d \quad (2)$$

where d is the optical path length. Hence, the absorbance spectrum was checked using a spectrophotometer (Tecan Infinite 200 PRO) for the stock solution and its dilutions. The standard deviation σ was calculated from the average of 334 points. The minimum detectable concentration (MDC) of nanoparticles was calculated as the average of the background signal plus 3σ. The contrast-to-noise ratio (CNR) [15] and the contrast (C) were employed as image quality parameters and estimated according to the following equations:

$$SNR = \frac{Signal - background}{\sqrt{\sigma_s^2 - \sigma_b^2}} \qquad C = \frac{Signal - background}{background}$$

where Signal (background) and σs (σb) are the average signal and its standard deviation in the ROI of the sample (background), respectively. The background signal was estimated at an ROI around the PE tube filled with MQ in the case of the *in vitro* setup and at an ROI around non-injected tissue in the *ex vivo* experiment. The PA images were analyzed with a *spectral unmixing* algorithm that allows for discrimination of the individual spectral profiles of a variety of sources, like fluorophores or dyes, in the case of spectral overlapping [15,16]. The acquired image was a matrix (M) of measured data ($w \times p$ array) that consisted of measurements at w different wavelengths, each containing a total of p pixels. This matrix can be expressed as the multiplication of two matrices: M = W · D, where W is the weighting matrix of the absorption spectra generated from the different components, and D is the matrix of their spatial distribution. Hence, with mathematical methods [17-19], it is possible to extract the matrix D and obtain the localization of the sources.

4. RESULTS AND DISCUSSION

5.

4.1 Synthesis and Bio-conjugation

The synthesis of 6-carboxypentylamido-hexanoic fluorescein succinimidyl ester was performed using a modification of the procedure reported by Wu and Fan for fluorescein derivatives [10]. In this method, condensation of the resorcinol and 4-carboxyphthalic anhydride in the presence of methanesulfonic acid produces a mixture of 5- and 6-carboxy-substituted fluorescein (Scheme S1 in SI). After protection of the hydroxyl groups with pivalic anhydride, pure 6-carboxy isomer(2) was obtained by crystallization of its diisopropylamine salt from ethanol. After removal of the diisopropylammonium cation, *N*-hydroxysuccinimide (NHS) was introduced as the reactive group for a subsequent reaction with the amine group of 6-amino hexanoic acid. The latter reaction leads to dipivaloyl-6-(5-carboxypentyl amino-carbonyl) fluorescein. After removal of the protecting pivalate groups by treatment with aqueous ammonia (NH3), the resulting 6-(5-carbo- xypentyl aminocarbonyl) fluorescein was finally treated with *N*-hydroxysuccinimidyl trifluoroacetate (NHS-TFA) to obtain the NHS ester, suitable for conjugation with the primary amines of the nanoparti- cles (for more information see “Synthesis and characterization” in SI).

4.2 Characterization of Magnetite Nanoshells (NBR)

Transmission electron microscopic images of nanoparticles are re- ported in Fig. 2. The mean hydrodynamic diameter and mean polydis- persity index (PDI) for the NBR were determined by dynamic light scattering and found to be 44.1 ± 1.6 nm and 0.17 ± 0.02, respectively, indicating a narrow size distribution. No major differences were de- tected for NBRfluo, which showed an average hydrodynamic diameter of 41.0 ± 0.6 nm and PDI = 0.13 ± 0.02. The ξ potentials of the two as- semblies of particles were − 41 mV and − 38 mV for NBR and NBRfluo, respectively, confirming their stability.

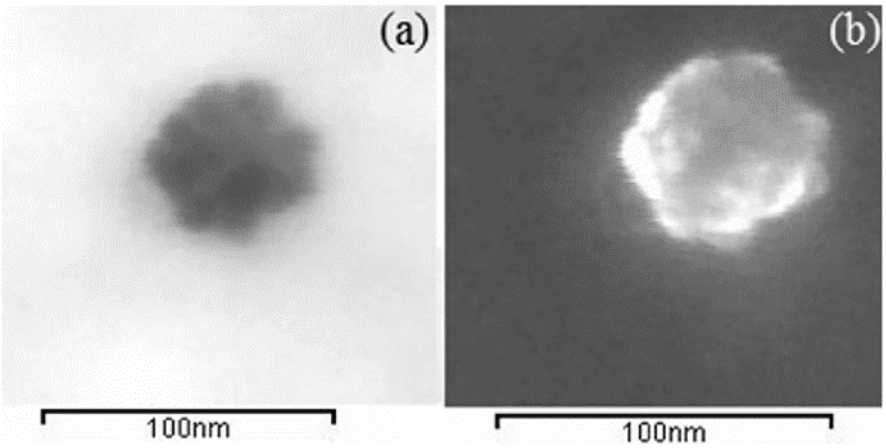

Fig. 2. Transmission (a) and scanning (b) electron micrographs of the NBR acquired with a Zeiss SUPRA™ 40 field emission scanning electron microscope (accelerating tension = 20 kV, aperture = 60 μm). Scale bar, 100 nm.

4.3 Spectroscopic Characterization

The 6-carboxypentylamido-hexanoic fluorescein succinimidyl ester presented the characteristic ultraviolet-visible (UV–Vis) absorption and emission spectra of the fluorescein fluorophore in its dianionic form (single bands at 491 nm and 518 nm, respectively, as reported in Fig. S1 in SI). In the case of the NBRfluo nanoparticles, the intrinsic ab- sorption of Fe3O4 overlapped with that of fluorescein, as well as with the scattering by nanoparticles, preventing the acquisition of a reliable absorption spectrum. However, the excitation and emission spectra presented the typical spectral features of fluorescein (a single band with peaks at 494 and 516 nm, respectively, as reported in Fig. S2 in SI). Spectrophotometric (SPH) results were obtained for the stock solution, diluted samples, and water (background). Typical absorbance patterns were measured in the PA optical window (Fig. 3, right) and exhibited a regular trend and intensity, suitable for providing a measurable PA signal. Different solutions of NBRfluo were prepared in order to estimate the image brightness in terms of optical absorbance and NBRfluo concentration. As a reference standard, methylene blue (MB) solutions were used as a comparison (Fig. 3, left).

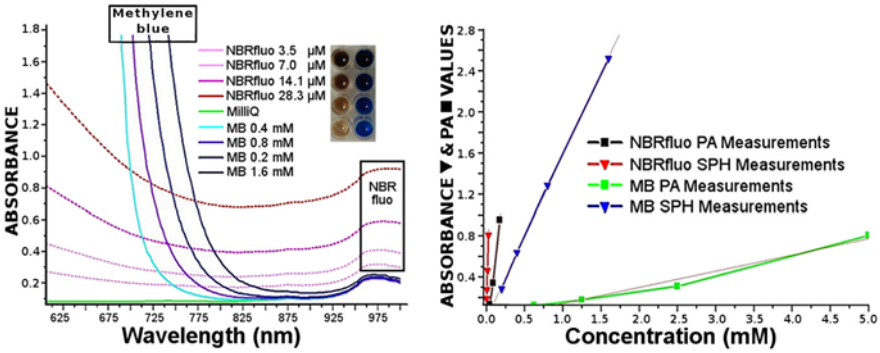

Fig. 3. Absorbance plot of different dilutions of MB and NBRfluo (left panel); linearity of PA- and SPH-acquired data with concentration (right panel).

4.4 PA Spectroscopic Analysis

PA spectroscopic analyses of phantoms containing five different solutions of NBRfluo in PE tubes were performed and found to provide a stable signal and a typical pattern, as shown in Fig. 4a. The typical spectral signal decreased until a wavelength of 740 nm, after which it remained constant until the end of the wavelength range (with standard deviations of 0.04, 0.03, 0.002, 0.04, and 0.05 arbitrary units at concentrations of 176.7 µM, 88.35 µM, 44.175 µM, 22.08 µM, and 11.04 µM, respectively); the magnitude of the slope decreased with the concentration in a second-order polynomial regression.

In order to investigate quenching, photo-bleaching [21], or reshaping phenomena [22], the PHSt of the nanoparticles was determined by irradiating freshly prepared samples of NBRfluo (in Fig. 4b was reported the trend of PA values acquired during time at 730 nm). The results showed high PHSt at all dilutions without any significant decrease in the PA signal; the brightness of each of the different dilutions inside the tubes was optically homogeneous. Although the nanoparticles displayed a detectable fluorescence, the strong PA signal indicated that radiative decay was moderate in these materials.

The relationship between the PA signal and the concentration of NBRfluo nanoparticles was extrapolated (Fig. 4c). There was a linear correlation between the two in the range of 44-176 µM, with a Pearson coefficient of approximately 0.996 (N0.7 indicates a strong correlation). The PA values are reported in Fig. 4e, and each of them was calculated over an average of 335 acquisitions. From the equation of linear fit and the PA background value (0.082 ± 0.007 a.u. at 730 m), the MDC of NBRfluo was calculated as 43 µM.

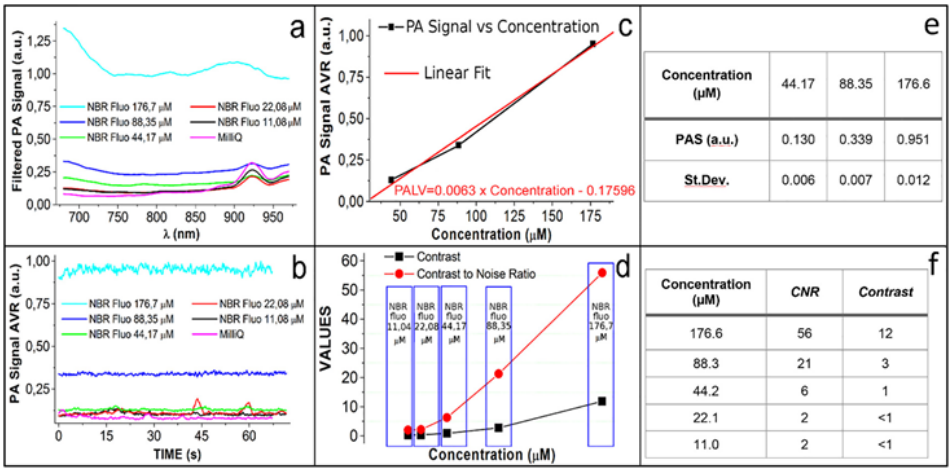

Fig. 4 (a) PA spectra of different dilutions of NBRfluo. At lower dilutions, a small PA spectral response of polyethylene (920 nm) is detectable; (b) PHSt under pulsed laser illumination at 730 nm; (c) Linearity fit of PA Signal *vs* Concentration; (d) CNR and Contrast trends; (e) Linearity plot values; (f) CNR and Contrast values.

The PA signal of NBRfluo was compared to those of the MB reference samples (Fig. 3, right), in which approximately 98% of the laser-absorbed energy was converted to heat [23]. The NBRfluo showed: 1) a PA signal higher than that of MB at the same concentration, 2) a good CNR (from 6 up to 56 at µM level, Fig. 4d,f), and 3) good stability, with very minimal fluctuation (Fig. 4e). The slope of the calibration curve is considered to indicate the system sensitivity (according to the International Union of Pure and Applied Chemistry, IUPAC), and its value was found to be 0.0063 (PA Signal/µM, Fig. 4c).

Fig. 5a shows a 3D PA rendering of a tube filled with stock solution; the 3D PA volume was determined at a fixed wavelength of 730 nm with motorized steps of 152 µm. As expected from the PHSt values, the PA response of the NBRfluo was stable and homogeneous across the entire length of the tube, implying that there was no precipitation. In Fig. 5b, the magnification of the (PA) frontal section of a PE tube filled with NBRfluo (176.7 µM) is shown, and Fig. 5c shows the same image processed with the spectral unmixing algorithm, which enables the discrimination of the specific PA spectral response of NBRfluo. Thus, the spectral unmixing analysis allows for the quantification of the PA signal generated from the nanoparticles specifically. As shown in Fig. 5c, the PA spectral responses of PE (yellow, 0.059 a.u.) and NBRfluo (green, 0.672 a.u.) were well discriminated in comparison to the total PA signal shown in Fig. 5b, in which the two PA signals overlapped.

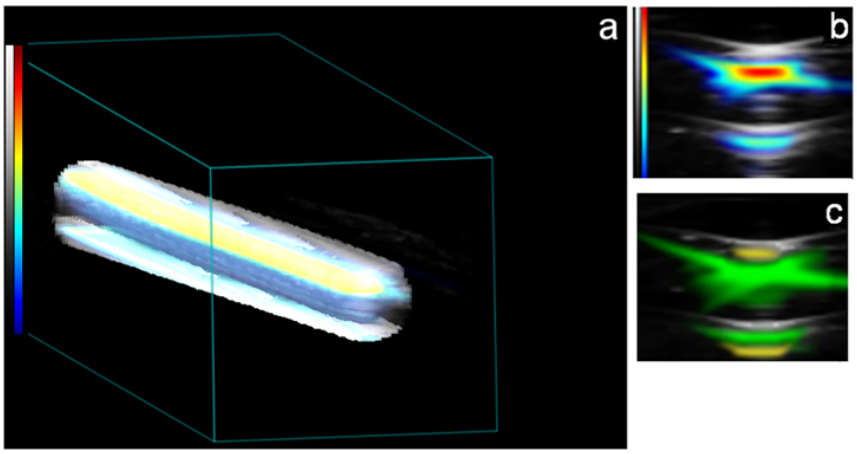

Fig. 5. . (a) Three-dimensional PA rendering of a tube filled with NBRfluo (176.7 μM); (b) PA image of a frontal section of the tube filled with NBRfluo (the intensity of the PA signal is shown as a colored gradient, and the intensity of the echographic signal is shown in grayscale); (c) PA image of the same tube section processed with the spectral unmixing algorithm showing the discrimination of different PA spectral responses: yellow, PE; green, NBRfluo.

The *ex vivo* PA spectrum of a chicken breast sample was recorded and is shown in Fig. 6a; approximately 100 μL of 176.7 μM NBRFluo was injected, and the nanoparticles were perfused into the muscle fibers (Fig. 6b,e). The typical PA signal was easily distinguished from the background, and the pattern of the entire PA spectrum was comparable to that detected previously (Fig. 4a). The stability trend exhibited minimal fluctuations with a standard deviation (SD) of 0.068 and a coefficient of variation (CV) of 0.024 (during 65 s of continuous pulsed laser irradiation at 830 nm) (Fig. 6d). The CNR obtained had a value of 41, and the Contrast value reached 30. The 3D PA allowed for fine dis- crimination of the different morphological regions, with an axial resolu- tion of 75 μm and lateral resolution of 165 μm (Fig. 6e).

The magnetic properties of the nanoparticles and their ability to modify the proton relaxation of water in the surrounding tissues through the modification of longitudinal (T1) and, in particular, transverse (T2) relaxation times are reported in SI. Good contrast properties of the NBR paramagnetic core, which enhances the proton relaxation (detectable in MRI), were observed, with the following values at 1.5 T: r_2 = 468.6 mM^{-1} s^{-1} and r_1 = 10.78 mM^{-1} s^{-1} (r_2/r_1 = 43.5). These values are comparable to those previously obtained with iron oxide negative contrast agents based on a magnetite core.

The optical imaging capabilities were also tested in the *ex vivo* phan- tom, and the results are reported in SI. These data help to demonstrate the limits of optical imaging and also confirm that the inherent resolu- tion limits of diffuse optical imaging can be overcome using PAI.

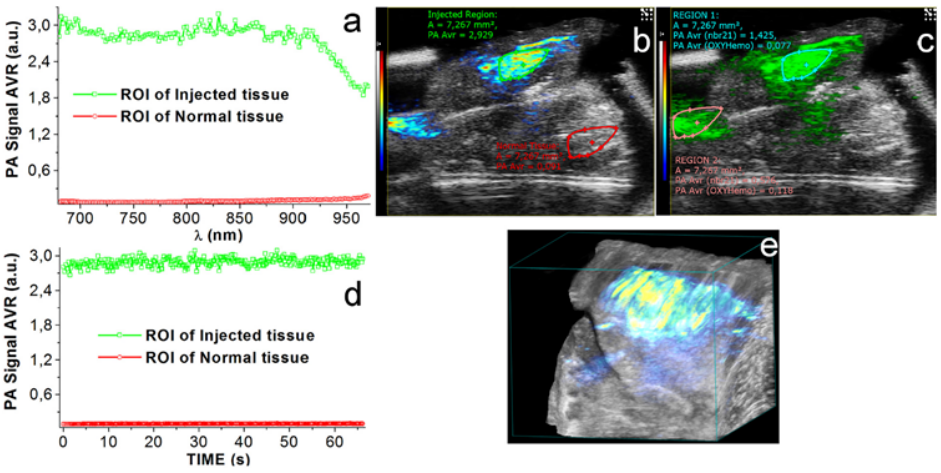

Fig.6. PA spectral analysis of injected chicken breast sample; (b) PA distribution in the injected region; (c) Spectral unmixing control, showing the discrimination of NBRfluo in the injected sample; (d) PHSt of injected and control regions of *ex vivo* chicken breast tissue under illumination; (e) 3D PA reconstruction of injected chicken breast sample.

5. Conclusion

We developed and tested a novel nanoshell by converting iron ox- ides into dual MRI/PAI probes with very good PA performance at the μM level when irradiated in the NIR region. Moreover, NBRfluo were detectable by MRI at 1.5 T, at which they showed good relaxivity values, indicating they are suitable for *in vivo* use. These results validate the ability of both imaging modalities to detect the multimodal-multifunctional nanoparticles. The high sensitivity provided by this nanoshell makes it a promising multimodal platform for biomarker development and bio-molecular imaging. Further studies on cell biocom- patibility and internalization are needed to fully exploit the PAI/MRI potential of these newly synthesized compounds for *in vivo* applica- tions, both for molecular imaging and cell-tracking studies.

LIST OF ABBREVIATIONS

C Contrast
CNR Contrast-to-noise ratio
CV Coefficient of variation
DMSO Dimethyl sulfoxide
ID Internal diameter
IUPAC International union of pure and applied chemistry
ED External diameter
NBR Nanobioreactor
NBRfluo Fluorescent nanobioreactor
NIR Near-infrared
MB Methylene blue
MDC Minimum detectable concentration
MQ MilliQ
MR Magnetic resonance
MRI Magnetic resonance imaging
NIR Near infrared
NH_3 Ammonia
NHS *N*-hydroxysuccinimide
NHS-TFA *N*-hydroxysuccinimidyl trifluoroacetate
OPO Optical parametric oscillator
OXY Oxygenated
PA Photoacoustic
PAI Photoacoustic Imaging
PALV Photoacoustic linearity values
PE Polyethylene
PHSt Photostability
PLGA-b-PEG-COOH carboxy-terminated poly(d,l-lactide-*co*-glycolide)-*block*-poly(ethylene glycol)
PDI Polydispersity index
ROI Region of interest
SD Standard deviation
SI Supplementary information
SPH Spectrophotometric
THF Tetrahydrofuran
UV–Vis Ultraviolet–visible

ACKNOWLEDGEMENTS

This project was co-financed under Tuscany POR FESR 2014-2020 Framework: project name “INSIDE” (CUP ST: 3389.30072014.067000001, years 2016-2018). We would like to thank Drs. F. Faita and N. Di Lascio for their contributions to image post-processing, and Dr. O. Crociani and Dr. M. Stefanini from the Di.v.a.l. Toscana center. We are also grateful to Fondazione CNR/Regione Toscana “G. Monasterio” for supporting these research activities.

REFERENCES

[1] N. Di Lascio, C. Avigo, P. Armanetti, F. Stea, L. Cavigli, F. Ratto, R. Pini, C. Kusmic, L. Menichetti, F. Faita, Pattern of distribution and kinetics of accumulation of gold nanorods in mouse spleen, Proc. SPIE 9323, Photons Plus Ultrasound: Imaging and Sensing 2015, 2015, p. 93234C

[2] M. Xu, L.V. Wang, Photoacoustic imaging in biomedicine, Rev. Sci. Instrum. 77 (2006), 041101.

[3] X. Wang, X. Xie, G. Ku, L.V. Wang, G. Stoica, Noninvasive imaging of hemoglobin concentration and oxygenation in the rat brain using high-resolution photoacoustic tomography, J. Biomed. Opt. 11 (2) (2006) 024015,

[4] H. Chen, Z. Yuan, C. Wu, Nanoparticle probes for structural and functional photo- acoustic molecular tomography, Biomed. Res. Int. 757101 (2015)

[5] D.L. Longo, R. Stefania, S. Aime, A. Oraevsky, Melanin-based contrast agents for bio- medical optoacoustic imaging and theranostic applications, Int. J. Mol. Sci. 18 (8) (2017) 1719

[6] C.J.H. Ho, G. Balasundaram, W. Driessen, R. McLaren, C.L. Wong, U.S. Dinish, A.B.E. Attia, V. Ntziachristos, M. Olivo, Multifunctional photosensitizer-based contrast agents for photoacoustic imaging, Sci. Rep. 4 (2014) 5342

[7] J. Weber, P.C. Beard, S.E. Bohndiek, Contrast agents for molecular photoacoustic im- aging, Nat. Methods 13 (8) (2016) 639–650.

[8] K. Pu, A.J. Shuhendler, J.V. Jokerst, J. Mei, S.S. Gambhir, Z. Bao, J. Rao, Semiconducting polymer nanoparticles as photoacoustic molecular imaging probes in living mice, Nat. Nanotechnol. 9 (3) (2014) 233–239.

[9] C. Avigo, A. Flori, P. Armanetti, N. Di Lascio, C. Kusmic, J. Jose, P. Losi, G. Soldani, F. Faita, L. Menichetti, Strategies for non-invasive imaging of polymeric biomaterial in vascular tissue engineering and regenerative medicine using ultrasound and pho- toacoustic techniques, Polym. Int. 65 (7) (2016) 734–740.

[10] G. Baldi, C. Ravagli, F. Mazzantini, G. Loudos, J. Adan, M. Masa, D. Psimadas, E. Fragogeorgi, E. Locatelli, C. Innocenti, C. Sangregorio, M. Comes Franchini, In vivo anti-cancer evaluation of hyperthermic efficacy of anti-hEGFR-targeted PEG-based nanocarrier containing magnetic nanoparticles, Int. J. Nanomedicine 9 (1) (2014) 3037–3056.

[11] C. Avigo, N. Di Lascio, P. Armanetti, C. Kusmic, L. Cavigli, F. Ratto, S. Meucci, C. Masciullo, M. Cecchini, R. Pini, F. Faita, L. Menichetti, Organosilicon phantom for photoacoustic imaging, J. Biomed. Opt. 20 (4) (2015), 046008.

[12] C. Avigo, P. Armanetti, C. Masciullo, N. Di Lascio, L. Cavigli, F. Ratto, R. Pini, M. Cecchini, C. Kusmic, F. Faita, L. Menichetti, Novel organosilicon phantoms as testing material for photoacoustic imaging, Proc. SPIE 9700, Design and Quality for Biomed- ical Technologies IX, 2016, p. 97000I.

[13] C. Avigo, N. Di Lascio, P. Armanetti, F. Stea, L. Cavigli, F. Ratto, R. Pini, S. Meucci, M. Cecchini, C. Kusmic, F. Faita, L. Menichetti, Phantom studies with gold nanorods as contrast agents for photoacoustic imaging: novel and old approaches, Proc. SPIE 9323, Photons Plus Ultrasound: Imaging and Sensing 2015, 2015, p. 93234B.

[14] Jun Xia, Junjie Yao, Lihong V. Wang, Photoacoustic Tomography: Principles and Ad- vances, Electromagnetic Waves (Cambridge, Mass.), Vol. 147, 2014 1–22.

[15] M.S. Patterson, F.S. Foster, The improvement and quantitative assessment of B-mode images produced by an annular array/cone hybrid, Ultrason. Imaging 5 (1983) 195–213.

[16] R.J. Paproski, A. Heinmiller, K. Wachowicz, R.J. Zemp, Multi-wavelength photoacous- tic imaging of inducible tyrosinase reporter gene expression in xenograft tumors, Sci. Rep. 4 (2014) 5329.

[17] G.P. Luke, D. Yeager, S.Y. Emelianov, Biomedical applications of photoacoustic imag- ing with exogenous contrast agents, Ann. Biomed. Eng. 40 (2) (2012) 422–437.

[18] L. Hervé, Nonnegative matrix factorization: a blind spectra separation method for in vivo fluorescent optical imaging, J. Biomed. Opt. 15 (5) (2010), 056009..

[19] A. Hyvärinen, J. Karhunen, E. Oja, Independent component analysis, Appl. Comput. Harmon. Anal. 21 (2001) 135–144.

[21] J. Laufer, E. Zhang, P. Beard, Evaluation of absorbing chromophores used in tissue phan- toms for quantitative photoacoustic spectroscopy and imaging, IEEE J. Sel. Top. Quan- tum Electron. 16 (3) (2010) 600–607.

[22] T.E. McGrath, A.C. Beveridge, G.J. Diebold, Laser-induced “regeneration” of colloidal particles: the effects of thermal inertia on the chemical reactivity of laser-heated particles, Angew. Chem. Int. Ed. Eng. 38 (22) (1999) 3353–3356.

[23] T. Stahl, T. Allen, P. Beard, Characterization of the thermalisation efficiency and photostability of photoacoustic contrast agents, Proc. SPIE 8943, Photons Plus Ultra- sound: Imaging and Sensing 2014, 2014, p. 89435H.